Materials Advances

ROYAL SOCIETY OF CHEMISTRY

PAPER

View Article Online
View Journal | View Issue

Cite this: *Mater. Adv.*, 2026, 7, 1303

First-principles investigation of sulfur and sulfur-oxide compounds as potential optically active defects on (6,5) SWCNT

Tina N. Mihm, *[a] Kasidet Jing Trerayapiwat,†[b] Xinxin Li,[cd] Xuedan Ma[ce] and Sahar Sharifzadeh [abfg]

Received 13th September 2025,
Accepted 13th December 2025

DOI: 10.1039/d5ma01054c

rsc.li/materials-advances

Semiconducting single-walled carbon nanotubes (SWCNT) functionalized with covalent defects are a promising class of optoelectronic materials with strong, tunable photoluminescence and demonstrated single photon emission (SPE). Here, we investigate sulfur-oxide containing compounds as a new class of optically active dopants on (6,5) SWCNT. Experimentally, it has been found that when the SWCNT is exposed to sodium dithionite, the resulting compound displays a red-shifted and bright photoluminescence peak that is characteristic of doping with covalent defects. We perform density functional theory calculations on the possible adsorbed compounds that may be the source of doping (S, SO, SO_2 and SO_3). We predict that the two smallest molecules strongly bind to the SWCNT with binding energies of ~1.5–1.8 eV and 0.56 eV for S and SO, respectively, and introduce in-gap electronic states into the bandstructure of the tube consistent with the measured red-shift of (0.1–0.3) eV, consistent with measurements. In contrast, the larger compounds are found to be either unbound or weakly physisorbed with no appreciable impact on the electronic structure of the tube, indicating that they are unlikely to occur. Overall, our study suggests that sulfur-based compounds are promising new dopants for (6,5) SWCNT with tunable electronic properties.

1 Introduction

Semiconducting single walled carbon nanotubes (SWCNT) doped with covalent defects display high purity single photon emission (SPE) with high quantum yields,[1–5] and show promise in technologies such as sensing[6–14] and quantum information science.[15,16] The controlled sensitivity of the SWCNT to adsorbates allows for a variety of covalent dopants to be introduced.[2,3,6,17,18] These dopants can induce new associated optical transitions observed as a red-shift in the optical spectrum,[1,2,4,5,17–21] and improved SPE.[3,16,18,20–24] due to either defect-induced symmetry breaking[20] or the presence of deep in-gap states.[25] As such, there is great interest in the discovery of new covalent defects that can be synthesized on SWCNT.

The most common covalent defects that have demonstrated SPE are atomic hydrogen[26] and oxygen,[2,5,11–13,20,23] and functionalized aryl molecules.[1,10,14,21,24,27–30] Both atomic and molecular defects result in a high intensity red-shift in the tube's photoluminescence. The aryl groups have the advantage of being more tunable through their functional groups,[1,16,21,24,27] but require careful control of the defect density to avoid excessive functionalization that results in exciton quenching.[3,31,32] Atomic defects are desirable because they are abundant and form at stable locations along the tube,[2,5,20,23] and, thus, may provide a practical path for industrial scale production of doped SWCNT. However, the degree of emission enhancement is generally lower for atomic defects compared to the aryl groups.[3]

Regardless of the defect type, SPE and optical properties are highly-dependent on the defect binding configuration.[18,20,33] Covalent defects are typically introduced to the SWCNT through breaking of one carbon sp^2 bond and attaching a ligand that creates an sp^3 defect site. For certain defects and adsorption sites, the defect forms an sp^2 bond to two carbon atoms, breaking a double bond but maintaining the sp^2 hybridization of the tube. The photoluminescence (PL) and photochromic properties of the tube strongly depend on the location of binding and the type of bond formed,[17,33,34] presumably due

[a] *Department of Electrical and Computer Engineering, Boston University, MA 02215, USA. E-mail: mihmtina@msu.edu, ssharifz@bu.edu*
[b] *Department of Chemistry, Boston University, Boston, MA 02215, USA*
[c] *Center for Nanoscale Materials, Argonne National Laboratory, Lemont, IL 60439, USA*
[d] *Consortium for Advanced Science and Engineering, University of Chicago, Chicago, IL 60637, USA*
[e] *Materials Science and NanoEngineering, Rice University, Houston, TX 77251, USA*
[f] *Materials Science Division, Boston University, Boston, MA 02215, USA*
[g] *Department of Physics, Boston University, Boston, MA 02215, USA*
† Present address: Center for Nanoscale Materials, Argonne National Laboratory, Lemont, IL 60439, USA.

to the varying degrees of perturbation to the SWCNT electronic structure.

In this article, we investigate sulfur and sulfur oxide (SO_x)-based sp^2 and sp^3 dopants as a class of atomic and small molecular covalent dopants that may be synthesized on (6,5) SWCNT. The (6,5) SWCNT is a chiral and semiconducting tube with clearly defined two lowest-energy optical transitions, E_{11} and E_{22} at $\sim$1.25 eV and $\sim$2.21 eV, respectively, with multiple optically-active dopants successfully introduced, including the oxygen atom.[2,5,11,12,20,23] In our study, sulfur and sulfur oxide-based defects were chosen as potential optically active defects because sulfur is isovalent to oxygen; thus, we expect similar bonding and optical properties associated with the sulfur doped SWCNT. Furthermore, when used to dope carbon materials, sulfur-containing compounds have shown efficient fluorescence quantum yield with tunable emissions,[35–38] indicating that sulfur may be an optically-active defect on (6,5) SWCNT. Experimentally, it was shown that introduction of sodium dithionite to solution-phase (6,5) SWCNT, which is expected to break down into SO_x (predominantly SO_2) on the surface, leads to a new doped species with the desired red-shifted strong emission.[39] Within density functional theory (DFT), we perform a comprehensive study of the most probable configurations of adsorbed SO_x that may arise (S, SO, SO_2, SO_3) in order to determine the most likely species that has been synthesized. We predict that the larger two molecules studied, SO_2 and SO_3, are weakly physisorbed to the SWCNT, with little to no electronic interaction to the tube, in agreement with prior DFT-based studies of these compounds on SWCNT.[40–47] In contrast, S and SO favorably and strongly bind to the tube with a red-shifted gap due to either defect-induced band splitting or introduction of an in-gap defect state. S in an sp^2 bonding configuration is predicted to be the most energetically stable configuration. Overall, our study indicates that S and SO defects can be incorporated into and tune the optical properties of (6,5) SWCNT.

The remainder of the paper is organized as follows: Section 2 outlines the DFT computational details and details of the binding configurations considered; Section 3 presents the predicted adsorbate binding energies, optimized structures, and electronic structure; Section 4 concludes with a statement on which SO_x defects are possibly the optically active defects that have been observed experimentally.

2 Computational methods

The electronic structure and adsorption energy of the pristine and doped SWCNT were computed within density functional theory (DFT) as implemented in the Vienna *Ab initio* Simulation Package (VASP),[48–52] with frozen-core projector-augmented wave (PAW) pseudopotentials describing the nuclei and core electrons.[53,54] The exchange–correlation was treated within the generalized gradient approximation (GGA) of Perdew, Burke, and Ernzerhof (PBE),[55] with the addition of Grimme D3 van der Waals corrections.[56] The choice of the PBE functional was made because empirical van der Waals corrections are better suited to PBE, which tends to underbind, rather than LDA, which tends to overbind.[57,58] We note that while GGA underestimates the band gap, our prior studies of aryl-doped (6,5) SWCNT found that while many-body corrections open up the gap, the relative energy between dopant and tube frontier states is consistent between LDA/GGA and many-body perturbation theory.[25] Tests performed using the hybrid HSE06 functional (see SI, Section S5)[59] indicated that HSE06 and PBE predict the same trend in binding energies as well as band energies, validating our choice to use the less computationally costly PBE functional.

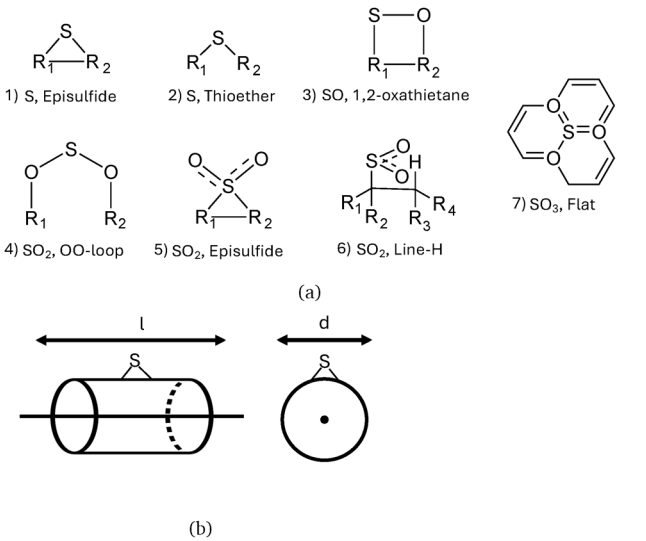

Fig. 1 (a) The configuration of different sulfur compounds studied relative to the carbon atoms of (6,5) SWCNT (labeled R_x). (b) Illustration of the two different orientations of the sulfur compounds relative to the SWCNT tube axis with a single sulfur atom shown as an example. The cylinder represents the (6,5) SWCNT.

All SWCNT were placed in a periodic cell with greater than 10 Å of vacuum along the two aperiodic directions. Restricted DFT calculations were performed for all but the passivated 'Line-H' SO_2 system (see Fig. 1(a)), which requires spin-polarized unrestricted DFT. Calculations were performed with a Γ-centered $1 \times 1 \times 2$ k-point mesh, which converged the total energy to less than 1 meV per atom (see SI, Section S6), and a plane wave energy cutoff of 400 eV, which is default for VASP. The structure of the full tube and defect were optimized until all forces were less than 0.01 eV $Å^{-1}$. The optimized lattice vector of the pristine (6,5) SWCNT is a = 32.4 Å, b = 20.0 Å, and c = 40.4 Å and was kept constant in the periodic direction (c) for all the defective systems.

The adsorbate binding energy was computed as

$$E_b = E_{CNT+SO_x} - (E_{CNT} + E_{SO_x}). \quad (1)$$

Here, the E_{CNT+SO_x} is the total energy of the adsorbate on SWCNT, E_{CNT} is the total energy of the pristine tube, and E_{SO_x} is the total energy of the sulfur compound in vacuum. To obtain the total energy of each system individually, all three were placed in a

box of the same size with the same computational parameters applied with the exception of the *k*-mesh for the isolated SO_x, which was $1 \times 1 \times 1$. For the hydrogen passivated SO_2 structure (structure 6 in Fig. 1(a)), we subtracted out the binding energy associated with the hydrogen atom (−1.41 eV), which did not interact with SO_2, from the total binding energy $\left(E_b^{SO_2+H} = -1.74 \text{ eV}\right)$. Thus, $E_b^{SO_2} = -1.74 \text{ eV} + 1.41 \text{ eV} = -0.31 \text{ eV}$.

We note that the experimental measurements were taken with the SWCNT suspended in solution of sodium dodecyl sulfate (SDS), which we do not account for in our simulations. These long carbon-chain surfactants have been shown to interact with aryl diazonium defects, with a noticeable impact on the selectivity of the dopant's binding configuration.[60,61] However, we expect this impact will be less significant for our atomic-scale defects. Exclusion of the surfactant is consistent with previous computational studies of oxygen and SO_2/SO_3 defects on SWCNT.[23,40–47] In addition, because the doped nanotubes are washed prior to analysis and the SO_x molecules are closed shell, we do not expect any charging of the dopant.

2.1 Structures studied

The different sulfur compounds considered and their corresponding binding configuration relative to the SWCNT are presented in Fig. 1(a). We study S, SO, SO_2, and SO_3 because it was previously determined that SO_2 may decompose into these compounds on SWCNT.[62] We considered different possible configurations of the adsorbate and only show configurations with favorable binding here; see SI Section S2.1 for details on unbound structures. The three kinds of covalent binding sites on the SWCNT are the sidewalls (side of tube), edge sites (end of tube), or near defects (such as vacancies and Stone–Wales complexes) Consistent with prior studies,[2,5,11,12,20,23] we considered only the sidewall because the edges make up a fraction of the surface area of the tube and would not result in the observed bright luminescence peak. We did not consider Stone–Wales defects because there was no evidence of the presence of these defects in experiment.[63,64] In order to test the impact of vacancies on the binding affinity, we studied the adsorption of the SO_2, line-H system in the vicinity of a single vacancy. The presence of the vacancy was found to cause SO_2 to become unbound, indicating that the vacancy does not enhance binding.

For the single sulfur atom, we considered epoxide-type and ether-type binding (structures 1 and 2), both of which have been shown to be energetically favorable locations for oxygen binding on (6,5) SWCNT.[23] In thioether-type bonding the S atom is arranged between a broken carbon–carbon bond resulting in sp^2 hybridization, while for episfulfide-type, the S atom sits between a single carbon–carbon bond with sp^3 hybridization. For the SO molecule, a four-member ring-type binding (structure 3) with the S and O each bound to one carbon atom was found to be favorable. For each S and SO configuration, we consider two different orientations of the C–S–C bonds, along the long ('l') and short ('d') axes of the tube (see Fig. 1(b)). We also considered two different 'l' placements for the thioether S structure, which are inequivalent due to the chiral symmetry of the (6,5) SWCNT: in-line with or offset from the tube's chirality (see Section S2.2 of the SI for structures). For SO_2, three different binding configurations were found to be favorable: (1) the SO_2 attached to two carbons across a broken carbon bond *via* the two oxygen on the SO_2 (structure 4), which was inspired by the orientation of SO_2 bound to graphene sheets and we label "OO-loop";[65,66] (2) the episulfide-type binding, a modification of the epoxide-type binding of S (structure 5); and (3) the SO_2 oriented such that the oxygen atoms are in line with a hydrogen atom that is attached to a carbon atom neighboring the adsorption site, labeled "line-H" (structure 6). The latter structure was introduced to test whether H can increase the affinity of the adsorbate to the tube. Lastly, for SO_3, a flat-type binding motivated by binding of SO_3 on graphene is found to be favorable (structure 7).[67]

3 Results and discussion

We investigate the possibility of doping (6,5) SWCNT with SO_x-based compounds by describing the binding and electronic structure of new compounds from first-principles calculations. The DFT-predicted binding energies of the sulfur-based compounds of Fig. 1 are presented in Table 1. The S atom is the most strongly bound to the tube, with binding energy ranging from −1.53 eV to −1.82 eV depending on the bonding arrangement. This value is greater than half of a C–S covalent bond energy of ∼−2.7 eV,[68,69] consistent with strong chemical bonding between the tube and S. The thioether-d configuration, which is the only structure studied that allowed the tube to retain its sp^2 hybridization, is the most strongly bound. Additionally, the binding is stronger along the short axis ('d') than along the long axis ('l') by 0.25–0.29 eV for the thioether and 0.12–0.16 eV for episulfide. This is consistent with previous studies of oxygen dopants on (6,5) SWCNT (see Table S.2 in the SI for comparison).[23] We note that the binding is slightly

Table 1 Calculated binding energy (E_b), the change in the energy difference between highest occupied and lowest unoccupied state upon adsorption (ΔE_{gap}), and shift in Fermi energy with respect to the pristine system (ΔE_f) for the defective (6,5) SWCNT configurations considered in this work. E_b is defined such that a negative energy is bound (see eqn (1)). All energies are in eV

Structure	E_b	ΔE_{gap}	ΔE_f
S, episulfide-d	−1.69	0.04	−0.04
S, thioether-d	−1.82	0.02	−0.01
S, episulfide-l Off-set with chiral direction	−1.53	0.28	0.05
S, episulfide-l In-line with chiral direction	−1.57	0.05	−0.03
SO, 1,2-oxathietane-l	−0.56	0.08	−0.07
SO,1,2-oxathietane-d	−0.56	0.08	−0.07
SO2, OO-loop-d	−0.20	0.00	−0.04
SO2, episulfide-d	−0.20	0.00	−0.05
SO2, line-H	−0.33	0.26	0.17
SO3, flat	−0.27	0.00	−0.08
Pristine	—	0.00	—
Experimental peak shift	—	0.12–0.26	—

stronger for the "l" position that is aligned with the tube's chirality compared with that off-line structure by 50 meV. Overall, these findings indicate that the binding of the sulfur on the CNT is influenced by its orientation, presumably due to the chiral nature of the tube.

For the SO_x molecules, binding is much weaker with binding energies <0.6 eV for all molecular configurations studied. The binding energy of the SO molecule is strongest at -0.56 eV for binding along both the long and short axes. SO_2 and SO_3 display much weaker binding to the surface, more consistent with physisorption. For SO_2, all configurations studied were predicted to bind *via* physisorption with energies ranging from -0.20 eV (no hydrogen) to -0.33 eV (with hydrogen), indicating that the presence of hydrogen only slightly enhances the bond strength. For SO_3, the binding energy is similarly weak at -0.27 eV. That the larger two defects, SO_2 and SO_3, are physisorbed on the surface is consistent with previous studies on carbon nanotubes.[40–46] The weaker binding for the SO_x molecules compared with a single sulfur atom can possibly be attributed to the fact that S–O bonds are already quite strong and stabilize the SO_x molecule, decreasing the molecule's affinity for forming new bonds. Additionally, the presence of oxygen makes the molecules larger and more bulky than with a single sulfur atom, with steric hindrance leading to a weaker SO_x bond compared to the sulfur atom.

To better understand the binding of SO_x to (6,5) SWCNT, we present the bonding arrangements of select compounds including bond lengths in Fig. 2 (see SI Table S.1 for all compounds). For the atomic S adsorbate, the bond length is 1.76–1.88 Å, close to the covalent bond length of $\sim$1.8 Å.[70] The bond angle between S and the two bonding carbons on tube (R_1 and R_2 in Fig. 1(a)) are 50.2°–66.4° (depending on orientation). The S–C bond is slightly stretched for SO adsorption ($\sim$2.05 Å) with the bond angles indicating a tilt towards one of the two carbons on the tube (S–R–R angle: $\sim$66° and $\sim$71°), which we attribute to steric effects due to the presence of the oxygen atom. The SO_2 and the SO_3 structures all have a predicted large adsorption distance of $\sim$3.0 Å away from the SWCNT, consistent with their weak binding. For SO_2, the bond angles for the OO-loop-d (S–R–R angle: 82.4° and 72.3°) and episulfide-d (S–R–R angle: 78.3° and 75.9°) structures indicate the molecule adsorbs slightly off of the C–C bond with S in the hollow site, while the hydrogen passivated structure shows the S in the SO_2 adsorbs on top of a carbon atom (S–R–R angle: 61.2° and 93.8°). The slight offset of the un-passivated SO_2 molecule from the carbon atoms may be attributed to steric effects between the SO_2 dipole and the SWCNT surface. SO_3 bond angles (S–R–R angle: 57.5° and 94.0°) also show adsorption of S on top of one of the carbons.

Next, we consider the impact of S, SO, SO_2, and SO_3 on the electronic structure of (6,5) SWCNT. Based on the predicted binding for the four compounds, we may expect that the S and SO defects will impact the bandstructure significantly due to their strong bond with the tube. Table 1 presents the energy gap between occupied and unoccupied states for all bound structures studies. The gap of the doped structures ranges from 0.64 eV to 0.92 eV, compared with the pristine tube gap of 0.92 eV. The strongly bound S and SO adsorbate always result in a reduced gap with respect to the pristine tube by 20–300 meV, indicating that the optical transitions will be red-shifted as a result of doping. This is in good agreement with experimental finding that the tube photoluminescence peak shifts by 100–300 meV upon exposure to sodium dithionate.[39] Table 1 also shows the shift in the Fermi energy of the tube upon doping. For all but two structures (with sulfur atoms in the "l" orientation), the shift is negative, indicating a slight negative charge transfer to the surface. However, the magnitude of all the differences is small, indicating weak doping.

Representative bandstructures for the tube doped with each defect type are shown in Fig. 3 with all bandstructures presented in the SI Fig. S6. The near-gap states of the (6,5) SWCNT are of π-type character with a two-fold degeneracy at $\mathbf{k} = 0$ due to the underlying graphitic structure. By inspection of the predicted bandstructures, we conclude that all of the defects studied break the symmetry of the tube, leading to splitting of the nearly-degenerate valence and conduction bands, consistent with

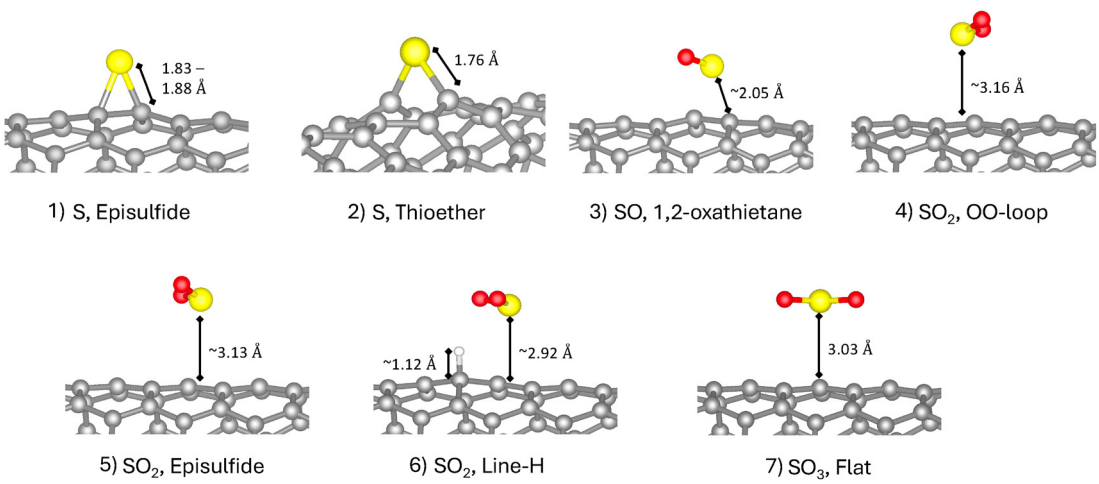

Fig. 2 The predicted adsorption geometry of SO_x derivatives on (6,5) SWCNT within PBE-D3. Relevant bond lengths are labeled.

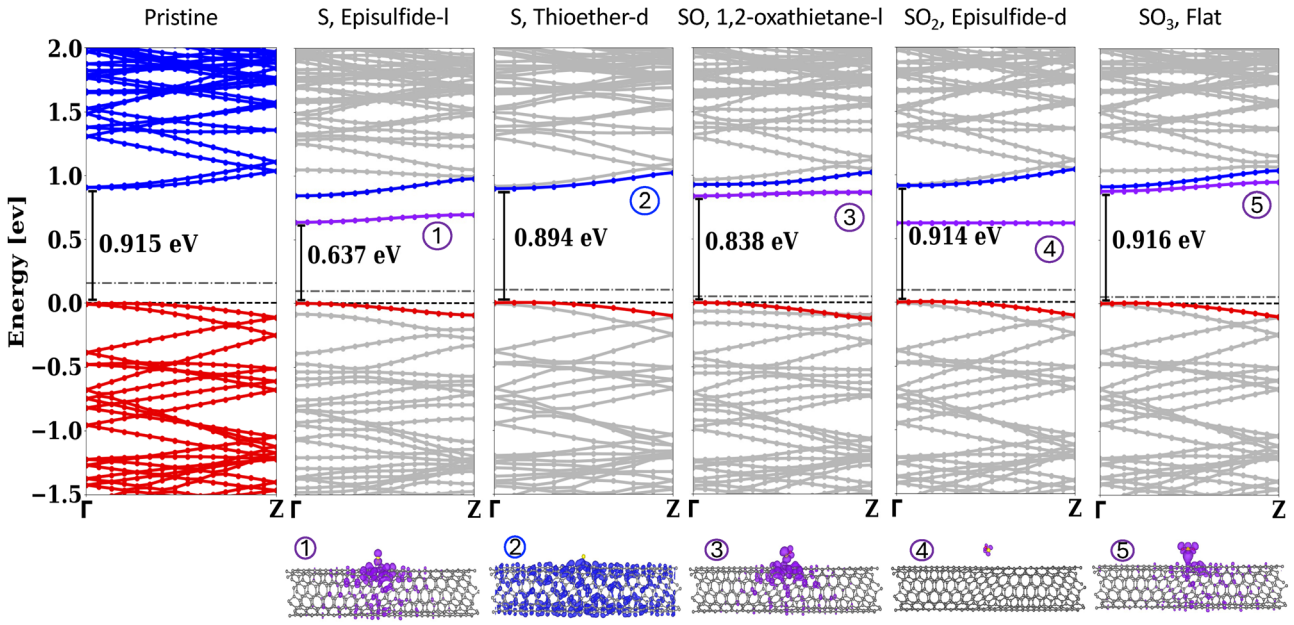

Fig. 3 PBE-predicted bandstructure for pristine (6,5) SWCNT and (6,5) SWCNT with the mostly likely adsorbate structures for S, SO, SO_2, and SO_3. Occupied pristine-like valence bands and unoccupied conduction bands are shown in red and blue, respectively, while unoccupied states localized on the defect are in purple. The gray dash-dot line on each band structure represents the Fermi energy. All plots are shifted such that the top of the pristine-like valence band is at zero at **k** = 0 (indicated by black dash line). The orbital charge density for the lowest energy unoccupied band is shown below the plots with an isosurface that captures 40% of the density.

previous reports for doped (6,5) SWCNT.[1,5,17,20,23,25–27] This splitting is largest for S and SO (see SI Fig. S.5 for more details). The maximum splitting within the conduction (valence) bands for episulfide-l S, thioether-d S, and SO are 200 meV (110 meV), 19 meV (9 meV) and 38 meV (67 meV), respectively. As noted previously for the oxygen dopant bound to SWCNT,[20] the ether-type bond maintains the sp^2 character of the tube and so the perturbation to the system is weaker than epoxide-type bonding, which creates an sp^3 bond on the tube. This weaker perturbation results in much smaller band splitting. The splitting of the bands for SO_2 is less than 4 meV for both valence and conduction bands, while for SO_3 it is 4 meV for the valence and 0.13 eV for the conduction band, consistent with the weaker interaction with the tube.

In addition to symmetry breaking-induced band splitting, both S and SO oriented along the long axis of the tube ('l' orientation) introduce a new unoccupied in-gap state associated with the defect into bandstructure, reducing the gap by up to 0.28 eV for S and 0.08 eV for SO. This in-gap state is associated with a localized defect-centered orbital hybridized with the SWCNT bands as shown in the orbital density plots below the bandstructure. This state is not present for S in the thioether-d configuration for which no defect-centered orbital is present near the gap. Interestingly, whether the defect is in-line with the chiral direction of the tube plays a role in the location of the in-gap state for the 'l'-oriented S defects: if the position of S is aligned with the tube's chirality the defect-centered state is significantly closer in energy to the conduction band.

SO_2 also introduces an in-gap state with an associated orbital density that is localized on the defect, indicating no interaction with the tube. For SO_3, there is an in-gap state resonant with the conduction bands. This state is slightly delocalized over parts of the tube and slightly dispersive. However, we suspect that this mixing between the defect state and conduction band may be artificial and due to DFT self-interaction error which results in mixing of two resonant states, as occurs in bond dissociation.[71]

Considering both the predicted binding energy and the change in the bandstructure upon adsorption, we expect that only S and SO are candidate covalent dopants to (6,5) SWCNT consistent with experiment with the most likely being a combination of the three sulfur atom configurations and a small amount of the SO dopants. These defects chemically bind to the SWCNT and result in in-gap states that decrease the band gap by 0.04–0.28 eV, consistent in energy with the red-shifted peaks in experiment at 0.12–0.26 eV (see Table 1). These transitions may be π–π^* excitations from symmetry broken band-edges configuration (as for the S atom in thioether-d) or may involve defect-localized in-gap unoccupied states (as for S in thioether-l configuration). We do not expect SO_2 or SO_3 to bind to the tube based on their weak adsorption energy. The fact that these larger molecules are physisorbed and do not impact the band-gap of the tube indicates that, even if they do bind, they do not contribute to the red-shifted PL.

Table S.2 compares the predicted binding energy and band gap reduction for our S/SO_x defects and other previously studied covalent defects. We note that compared to oxygen, for which the adsorption energy varies by >1 eV depending on the adsorption site (see Table S.2), the sulfur binding sites are quite close in energy. Thus, we expect sulfur to bind across the

different binding sites of the SWCNT, which we predict will have differing electronic transitions from their associated banstructure shown in Fig. 3. This prediction is consistent with the increased structure and broadening in the PL spectrum of sulfur-doped SWCNT compared with the oxygen-doped tube.

Lastly, we note that while the exact binding energies and red-shift of the gap depends on the level of theory considered, we expect the trends to be consistent among different levels of theory, as evidenced by select calculations presented in Table S.3.

Overall, we determine that the binding of the dopant to the SWCNT disrupts the carbon sp^2 bonds, with the perturbation causing the red-shift seen in the PL spectrum. For the large defects that physisorb on the tube, the disruption is minimal, while for the chemically bound SO and S atoms, the impacts is significant and observable.

4 Conclusions

In summary, DFT calculations were used to understand the binding of sulfur-based covalent defects on (6,5) SWCNT. We performed DFT calculations of the adsorption energy and bandstructure of four possible SO_x defects (S, SO, SO_2, and SO_3) onto (6,5) SWCNT. We determined that the two smaller defects, S and SO are strongly bound, with bond distances consistent with a carbon–sulfur covalent bond. In addition, there is a strong dependence of binding energy on the adsorption location along the tube. Furthermore, we predict S in the sp^2 hybridized thioether-d position is the most strongly bound at 1.8 eV and therefore most likely to form, reducing the gap by $\sim$20 meV, slightly smaller than the red-shift of the bright peak in experiment. S in the sp^3 hybridized episulfide-l is also strongly bound and red-shifts the bandgap by up to 0.3 eV, consistent with the observed low-energy shoulder in the PL spectrum. SO is also strongly bound to the CNT by 0.56 eV and red-shifts the gap by 80 meV, consistent with the brightest peak in the PL spectrum. Our analysis indicates that both S and SO have potential for use as an emissive defect for use in tuning the photoluminescence energy of the SWCNT and may be able to form through the synthetic technique given in ref. 39.

Author contributions

Tina N. Mihm – conceptualization (equal); formal analysis (lead); investigation (lead); visualization; writing – original draft preparation (equal); writing – review and editing (equal). Kasidet Jing Trerayapiwat – investigation (supporting); writing – review and editing (equal); resources. Xinxin Li – investigation (supporting); formal analysis (supporting); writing – review and editing (equal). Xuedan Ma – conceptualization (lead); supervision (lead); writing – review and editing (equal). Sahar Sharifzadeh – conceptualization (lead); supervision (lead); writing – original draft preparation (equal); writing – review and editing (equal).

Conflicts of interest

The authors have no conflicts to disclose.

Data availability

Data for this article, including inputs and outputs for all VASP calculations are available at SO_x-CNT at https://github.com/fpmats/Calculation_IO/tree/main/SOx-CNT. All other data supporting this article have been included as part of the main text and supplementary information (SI). Supplementary information: measured spectrum of the doped SWCNT, additional binding information on the SO_x adsorbates including unbound structures, examples of the binding configurations for the two thioether-l positions, and a table of all bond lengths and bond angles for each adsorbate. We also provide charge density differences and a graph of the band splitting across *k*-points for the five defects shown in Fig. 4 in the text, along with all band structures and projected density of states for all adsorbates studied. Finally, we provide a comparison of our new covalent defects against previously studied covalent defects, a comparison of PBE results *vs.* HSE06 and GW/BSE approximation for pristine and one dopant, and *k*-point convergence testing results. See DOI: https://doi.org/10.1039/d5ma01054c.

Acknowledgements

S. S. and T. M. acknowledge financial support from the U.S. Department of Energy (DOE), Office of Science, Basic Energy Sciences under Award No. DE-SC0023402. We also acknowledge support from the National Science Foundation under award no. DMR-2421596 and EECS-2427198. X. M. acknowledges support from the Air Force Office of Scientific Research under award number FA9550-25-1-0068. Work performed at the Center for Nanoscale Materials, a U.S. Department of Energy Office of Science User Facility, was supported by the U.S. DOE, Office of Basic Energy Sciences, under Contract No. DE-AC02-06CH11357. We would like to acknowledge computational resources from the National Energy Research Scientific Computing Center (NERSC), a DOE Office of Science User Facility supported by the Office of Science of the U.S. Department of Energy under Contract No. DE-AC02-05CH11231, and Boston University's Research Computing Services.

Notes and references

1 Y. Piao, B. Meany, L. R. Powell, N. Valley, H. Kwon, G. C. Schatz and Y. Wang, *Nat. Chem.*, 2013, **5**, 840–845.
2 X. Ma, N. F. Hartmann, J. K. S. Baldwin, S. K. Doorn and H. Htoon, *Nat. Nanotechnol.*, 2015, **10**, 671–675.
3 Q. H. Wang and M. S. Strano, *Nat. Chem.*, 2013, **5**, 812–813.
4 X. He, L. Sun, B. J. Gifford, S. Tretiak, A. Piryatinski, X. Li, H. Htoon and S. K. Doorn, *Nanoscale*, 2019, **11**, 9125–9132.
5 Y. Miyauchi, M. Iwamura, S. Mouri, T. Kawazoe, M. Ohtsu and K. Matsuda, *Nat. Photonics*, 2013, **7**, 715–719.

6 P. W. Barone, S. Baik, D. A. Heller and M. S. Strano, *Nat. Mater.*, 2005, **4**, 86–92.
7 S. Settele, C. A. Schrage, S. Jung, E. Michel, H. Li, B. S. Flavel, A. S. K. Hashmi, S. Kruss and J. Zaumseil, *Nat. Commun.*, 2024, **15**, 706.
8 P. Galonska, J. M. Mohr, C. A. Schrage, L. Schnitzler and S. Kruss, *J. Phys. Chem. Lett.*, 2023, **14**, 3483–3490.
9 J. T. Metternich, J. A. C. Wartmann, L. Sistemich, R. Nißler, S. Herbertz and S. Kruss, *J. Am. Chem. Soc.*, 2023, **145**, 14776–14783.
10 A. Spreinat, M. M. Dohmen, J. Lüttgens, N. Herrmann, L. F. Klepzig, R. Nißler, S. Weber, F. A. Mann, J. Lauth and S. Kruss, *J. Phys. Chem. C*, 2021, **125**, 18341–18351.
11 S. Basu, A. Hendler-Neumark and G. Bisker, *ACS Nano*, 2024, **18**, 34134–34146.
12 S. Basu, A. Hendler-Neumark and G. Bisker, *J. Phys. Chem. Lett.*, 2024, **15**, 10425–10434.
13 C.-W. Lin, S. M. Bachilo, Y. Zheng, U. Tsedev, S. Huang, R. B. Weisman and A. M. Belcher, *Nat. Commun.*, 2019, **10**, 2874.
14 F. A. Mann, N. Herrmann, F. Opazo and S. Kruss, *Angew. Chem., Int. Ed.*, 2020, **59**, 17732–17738.
15 A. Högele, C. Galland, M. Winger and A. Imamoğlu, *Phys. Rev. Lett.*, 2008, **100**, 217401.
16 X. He, H. Htoon, S. K. Doorn, W. H. P. Pernice, F. Pyatkov, R. Krupke, A. Jeantet, Y. Chassagneux and C. Voisin, *Nat. Mater.*, 2018, **17**, 663–670.
17 B. M. Weight, A. E. Sifain, B. J. Gifford, D. Kilin, S. Kilina and S. Tretiak, *J. Phys. Chem. Lett.*, 2021, **12**, 7846–7853.
18 J. Zaumseil, *Adv. Opt. Mater.*, 2022, **10**, 2101576.
19 X. Wang and T. C. Berkelbach, *J. Chem. Theory Comput.*, 2020, **16**, 3095–3103.
20 S. Ghosh, S. M. Bachilo, R. A. Simonette, K. M. Beckingham and R. B. Weisman, *Science*, 2010, **330**, 1656–1659.
21 X. He, N. F. Hartmann, X. Ma, Y. Kim, R. Ihly, J. L. Blackburn, W. Gao, J. Kono, Y. Yomogida, A. Hirano, T. Tanaka, H. Kataura, H. Htoon and S. K. Doorn, *Nat. Photonics*, 2017, **11**, 577–582.
22 S.-H. Lohmann, K. J. Trerayapiwat, J. Niklas, O. G. Poluektov, S. Sharifzadeh and X. Ma, *ACS Nano*, 2020, **14**, 17675–17682.
23 X. Ma, L. Adamska, H. Yamaguchi, S. E. Yalcin, S. Tretiak, S. K. Doorn and H. Htoon, *ACS Nano*, 2014, **8**, 10782–10789.
24 A. Ishii, X. He, N. F. Hartmann, H. Machiya, H. Htoon, S. K. Doorn and Y. K. Kato, *Nano Lett.*, 2018, **18**, 3873–3878.
25 K. J. Trerayapiwat, X. Li, X. Ma and S. Sharifzadeh, *Nano Lett.*, 2024, **24**, 667–671.
26 S. Kilina, J. Ramirez and S. Tretiak, *Nano Lett.*, 2012, **12**, 2306–2312.
27 N. F. Hartmann, S. E. Yalcin, L. Adamska, E. H. Hároz, X. Ma, S. Tretiak, H. Htoon and S. K. Doorn, *Nanoscale*, 2015, **7**, 20521–20530.
28 B. M. Weight, B. J. Gifford, S. Tretiak and S. Kilina, *J. Phys. Chem. C*, 2021, **125**, 4785–4793.
29 A. Setaro, M. Adeli, M. Glaeske, D. Przyrembel, T. Bisswanger, G. Gordeev, F. Maschietto, A. Faghani, B. Paulus, M. Weinelt, R. Arenal, R. Haag and S. Reich, *Nat. Commun.*, 2017, **8**, 14281.
30 K. Hayashi, Y. Niidome, T. Shiga, B. Yu, Y. Nakagawa, D. Janas, T. Fujigaya and T. Shiraki, *Chem. Commun.*, 2022, **58**, 11422–11425.
31 M. Sander, J. Metternich, P. Dippner, S. Kruss and L. Borchardt, *Controlled Introduction of sp3 quantum defects in Fluorescent Carbon Nanotubes by Mechanochemistry*, 2024, https://chemrxiv.org/engage/chemrxiv/article-details/671f2dee83f22e42146a3ad6.
32 N. Karousis, N. Tagmatarchis and D. Tasis, *Chem. Rev.*, 2010, **110**, 5366–5397.
33 B. J. Gifford, S. Kilina, H. Htoon, S. K. Doorn and S. Tretiak, *J. Phys. Chem. C*, 2018, **122**, 1828–1838.
34 S. Settele, F. J. Berger, S. Lindenthal, S. Zhao, A. A. El Yumin, N. F. Zorn, A. Asyuda, M. Zharnikov, A. Högele and J. Zaumseil, *Nat. Commun.*, 2021, **12**, 2119.
35 Z. Liu, C. Shan, G. Wei, J. Wen, L. Jiang, G. Hu, Z. Fang, T. Tang and M. Li, *Molecules*, 2023, **28**, 3637.
36 K. Luo, W. Sun, Y. Chi, S. Chai, C. Sun and W. Wu, *J. Mol. Struct.*, 2023, **1294**, 136525.
37 G. Ma, G. Ning and Q. Wei, *Carbon*, 2022, **195**, 328–340.
38 M. Jin, S. Lee, S. B. Lim, M. Lee, J. Park, H.-D. Jung, M.-H. Kang and K. Na, *Small*, 2025, **21**, 2410765.
39 X. Li, T. N. Mihm, J.-S. Chen, H. Hou, J. Wen, S. Sharifzadeh and X. Ma, *J. Phys. Chem. C*, 2025, **129**, 17590–17598.
40 Y. Chen, S. Yin, Y. Li, W. Cen, J. Li and H. Yin, *Appl. Surf. Sci.*, 2017, **404**, 364–369.
41 S. Yu and W. Yi, *IEEE Trans. Nanotechnol.*, 2007, **6**, 545–548.
42 M. Mittal and A. Kumar, *Sens. Actuators, B*, 2014, **203**, 349–362.
43 F. Yao, D. L. Duong, S. C. Lim, S. B. Yang, H. R. Hwang, W. J. Yu, I. H. Lee, F. Güneş and Y. H. Lee, *J. Mater. Chem.*, 2011, **21**, 4502–4508.
44 A. Goldoni, R. Larciprete, L. Petaccia and S. Lizzit, *J. Am. Chem. Soc.*, 2003, **125**, 11329–11333.
45 S. Peymani, M. Izadyar and A. Nakhaeipour, *Phys. Chem. Res.*, 2016, **4**, 553–565.
46 M. Oftadeh, M. Gholamian and H. H. Abdallah, *Phys. Chem. Res.*, 2014, **2**, 30–40.
47 W. Shen, F. Li, C. Liu and L.-C. Yin, *Chem. Phys. Lett.*, 2014, **608**, 1–5.
48 G. Kresse and J. Furthmüller, *Phys. Rev. B:Condens. Matter Mater. Phys.*, 1996, **54**, 11169–11186.
49 G. Kresse and J. Furthmüller, *Comput. Mater. Sci.*, 1996, **6**, 15–50.
50 G. Kresse and J. Hafner, *Phys. Rev. B:Condens. Matter Mater. Phys.*, 1993, **47**, 558–561.
51 G. Kresse and J. Hafner, *Phys. Rev. B:Condens. Matter Mater. Phys.*, 1994, **49**, 14251–14269.
52 G. Kresse and J. Hafner, *J. Phys.: Condens. Matter*, 1994, **6**, 8245–8257.
53 P. E. Blöchl, *Phys. Rev. B:Condens. Matter Mater. Phys.*, 1994, **50**, 17953–17979.
54 G. Kresse and D. Joubert, *Phys. Rev. B:Condens. Matter Mater. Phys.*, 1999, **59**, 1758–1775.

55 J. P. Perdew, K. Burke and M. Ernzerhof, *Phys. Rev. Lett.*, 1996, **77**, 3865–3868.
56 S. Grimme, J. Antony, S. Ehrlich and H. Krieg, *J. Chem. Phys.*, 2010, **132**, 154104.
57 L. He, F. Liu, G. Hautier, M. J. T. Oliveira, M. A. L. Marques, F. D. Vila, J. J. Rehr, G.-M. Rignanese and A. Zhou, *Phys. Rev. B:Condens. Matter Mater. Phys.*, 2014, **89**, 064305.
58 P. Haas, F. Tran and P. Blaha, *Phys. Rev. B:Condens. Matter Mater. Phys.*, 2009, **79**, 085104.
59 A. V. Krukau, O. A. Vydrov, A. F. Izmaylov and G. E. Scuseria, *J. Chem. Phys.*, 2006, **125**, 224106.
60 X. He, B. J. Gifford, N. F. Hartmann, R. Ihly, X. Ma, S. V. Kilina, Y. Luo, K. Shayan, S. Strauf, J. L. Blackburn, S. Tretiak, S. K. Doorn and H. Htoon, *ACS Nano*, 2017, **11**, 10785–10796.
61 A. J. Hilmer, T. P. McNicholas, S. Lin, J. Zhang, Q. H. Wang, J. D. Mendenhall, C. Song, D. A. Heller, P. W. Barone, D. Blankschtein and M. S. Strano, *Langmuir*, 2012, **28**, 1309–1321.
62 A. Goldoni, L. Petaccia, L. Gregoratti, B. Kaulich, A. Barinov, S. Lizzit, A. Laurita, L. Sangaletti and R. Larciprete, *Carbon*, 2004, **42**, 2099–2112.
63 G. Yu and L. Wang, *Phys. B*, 2023, **667**, 415143.
64 T. Biktagirov, U. Gerstmann and W. G. Schmidt, *Nanoscale*, 2025, **17**, 6884–6891.
65 E. Humeres and R. D. F. P. M. Moreira, *J. Phys. Org. Chem.*, 2012, **25**, 1012–1026.
66 E. Humeres, N. A. Debacher, R. D. F. P. M. Moreira, J. A. Santaballa and M. Canle, *J. Phys. Chem. C*, 2017, **121**, 14649–14657.
67 A. Shokuhi Rad, M. Esfahanian, S. Maleki and G. Gharati, *J. Sulfur Chem.*, 2016, **37**, 176–188.
68 *Covalent Bond Energies*, https://gchem.cm.utexas.edu/data/section2.php?target=bond-energies-table4.php.
69 Fundamentals of Chemical Bonding, 2013, https://chem.libretexts.org/Bookshelves/Physical_and_Theoretical_Chemistry_Textbook_Maps/Supplemental_Modules_(Physical_and_Theoretical_Chemistry)/Chemical_Bonding/Fundamentals_of_Chemical_Bonding.
70 W. Haynes, *CRC Handbook of Chemistry and Physics*, CRC Press, 2016.
71 A. Ruzsinszky, J. P. Perdew, G. I. Csonka, O. A. Vydrov and G. E. Scuseria, *J. Chem. Phys.*, 2006, **125**, 194112.